

SIMULATING THE BEHAVIOR OF SOFT COHESIVE SOILS USING THE GENERALIZED BOUNDING SURFACE MODEL

*Victor N. Kaliakin*¹, *Andres Nieto-Leal*²

¹University of Delaware, Newark, USA

²Universidad Militar Nueva Granada, Cajica, COLOMBIA

Abstract: The Generalized Bounding Surface Model (GBSM) for saturated cohesive soils is a fully three-dimensional, time and temperature-dependent model that accounts for both inherent and stress induced anisotropy. To better simulate the behavior of cohesive soils exhibiting softening, the model employs a non-associative flow rule. The GBSM synthesizes many previous bounding surface constitutive models for saturated cohesive soils and improves upon their predictive capabilities. For those cases where the use of the more complex forms of the GBSM is not justified, the model can be adaptively changed to simpler forms, thus reducing the number of associated parameters, giving flexibility to the simulations and reducing the computational cost. Following a brief overview of the GBSM, the model's performance in simulating the response of soft, saturated cohesive soils is assessed under both axisymmetric and true triaxial conditions.

Keywords: bounding surface, elastoplasticity, viscoplasticity, cohesive soils, soft soils

МОДЕЛИРОВАНИЕ ПОВЕДЕНИЯ МЯГКИХ КОГЕТИЧЕСКИХ ПОЧВ С ИСПОЛЬЗОВАНИЕМ ОБОБЩЕННОЙ МОДЕЛИ ОБЪЕМНОЙ ПОВЕРХНОСТИ

*В.Н. Калякин*¹, *Андрес Ньето-Лил*²

¹ Университет штата Делавэр, г. Ньюарк, США

² Университет Милитара Нуэва, г. Кахика, КОЛУМБИЯ

Аннотация: Обобщенная модель ограничивающей поверхности (GBSM) для насыщенных связных почв является полностью трехмерной моделью, зависящей от времени и температуры, которая учитывает как собственную, так и вызванную напряжением анизотропию. Чтобы лучше моделировать поведение связных почв, проявляющих размягчение, модель использует неассоциированное правило потока. GBSM синтезирует многие предыдущие модели ограничивающей поверхности для насыщенных связных грунтов и улучшает их прогнозные возможности. Для тех случаев, когда использование более сложных форм GBSM неоправданно, модель может быть адаптивно изменена на более простые формы, тем самым уменьшая количество связанных параметров, обеспечивая гибкость моделирования и уменьшая вычислительные затраты. После краткого обзора GBSM эффективность модели при моделировании реакции мягких, насыщенных связных грунтов оценивается как в осесимметричных, так и в истинных трехосных условиях.

Ключевые слова: ограничивающая поверхность, упругопластичность, вязкопластичность, связные грунты, мягкие грунты

1. INTRODUCTION

The Generalized Bounding Surface Model (GBSM) synthesizes many previous bounding surface constitutive models for saturated cohesive soils and improves upon their simulative and predictive capabilities. In a recent paper [1], a detailed description of the

GBSM was presented. Although some model simulations were also presented, they were, out of necessity, rather general in scope. As such, this paper supplements the earlier work [1]. Following a brief overview of the bounding surface concept and the GBSM, the model's performance in simulating the response of soft, saturated cohesive soils is assessed.

2. THE BOUNDING SURFACE CONCEPT IN STRESS SPACE

Some general aspects of the bounding surface concept in stress space are presented in this section. Additional details pertaining to theoretical aspects of this concept are given by Dafalias [2]; Kaliakin et al. [1] present a more specialized discussion of the concept as it applies to the GBSM. In the subsequent development tensorial quantities are presented in indicial form with the indices obeying the summation convention over repeated indices.

The material state is defined in terms of effective stresses σ'_{ij} and a set of proper internal variables q_n that embody the past loading history. In the subsequent development tensorial quantities are presented in indicial form with the indices obeying the summation convention over repeated indices. The single subscript on the q_n is not a tensorial index but denotes the plurality of these internal variables.

The existence of a smooth and convex bounding surface in effective stress space is assumed [2,3]. The surface always encloses the origin and is origin-convex; i.e., any radius emanating from the origin intersects the surface at only one point (Figure 1). Similar to a yield surface, the bounding surface is analytically given by

$$F(\bar{\sigma}'_{ij}, q_n) = 0 \quad (1)$$

where $\bar{\sigma}'_{ij}$ indicates an “image” point on the bounding surface. The actual stress point σ'_{ij} always lies within or on the surface. To each σ'_{ij} a unique $\bar{\sigma}'_{ij}$ is assigned by a properly defined “mapping” rule that becomes the identity mapping if σ'_{ij} lies on the bounding surface (i.e., if $\sigma'_{ij} = \bar{\sigma}'_{ij}$) [2].

Dafalias [4] introduced a very simple “radial mapping” form of the model that does not require an explicit definition of a yield surface.

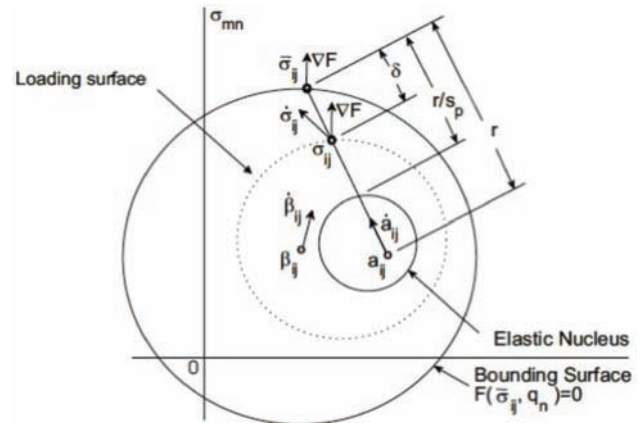


Figure 1. Schematic illustration of the bounding surface, a loading surface and radial mapping rule in multiaxial stress space.

In the radial mapping form of the model, shown schematically in Figure 1, it is assumed that the projection center a_{ij} lies always within the bounding surface and never crosses it. The a_{ij} evolves according to a proper rate equation, and is one of the q_n . It does not, however, enter into equation (1). Using a_{ij} as the projection center, the “image” stress is obtained by the radial projection of the actual stress (σ'_{ij}) onto the surface according to the following mapping rule:

$$\bar{\sigma}'_{ij} = b (\sigma'_{ij} - a_{ij}) + a_{ij} \quad (2)$$

which becomes the identity mapping if σ'_{ij} is on the surface (Figure 1). The dimensionless positive parameter b ($1 \leq b \leq \infty$) is determined in terms of the material state by substituting the “image” stress from equation (2) into an explicit form of equation (1), and solving the resulting expression for b .

The essence of the bounding surface concept is the hypothesis that inelastic deformations can occur for stress states either within or on a properly defined bounding surface. The extent of these deformations depends on the Euclidean distance δ between σ'_{ij} and an associated “image” stress that is defined using equation (2). Thus, unlike classical yield surface elastoplasticity, inelastic states are not restricted only to those lying on an outer loading or bounding surface [2].

To complete the formulation, a general state-dependent relation between the plastic modulus K_p (associated with the actual stress point) and the “bounding” plastic modulus \bar{K}_p associated “image” stress points must be established as a function of the properly chosen distances δ and r shown in Figure 1 according to

$$K_p = \bar{K}_p + \hat{H}(\sigma'_{ij}, q_n) \frac{\delta}{\langle r - s_p \delta \rangle} \quad (3)$$

where r can be related to b through the relation

$$r/\delta = b/(b - 1).$$

The “bounding” plastic modulus is obtained from the consistency condition; i.e., $\dot{F} = 0$. In equation (3), s_p (≥ 1.0) is a model parameter that defines the extent of the elastic nucleus (a region of purely elastic response), such that $(r - s_p \delta) \geq 0$ (Figure 1), and the dimensionless parameter $b \geq 1.0$ is as previously defined. The quantity \hat{H} denotes a proper scalar shape hardening function of the state that is independent of the explicit form of equation (1). The exact definition of \hat{H} requires the identification and experimental determination of certain material parameters [5]. Finally, the symbols $\langle \rangle$ denote Macaulay brackets, which imply that, for some quantity d ,

$$\langle d \rangle = d \text{ if } d > 0 \text{ and } \langle d \rangle = 0 \text{ if } d \leq 0.$$

Equation (3), which is by no means unique, embodies the meaning of the bounding surface concept. If $\delta < r$ and \hat{H} is not approaching infinity, the concept allows for plastic deformations to occur for points either within or on the surface at a progressive pace that depends upon δ . The closer to the bounding surface is the actual stress point (σ'_{ij}), the smaller is K_p (it approaches the corresponding “bounding” plastic modulus), and the greater is the plastic strain increment for a given stress increment. Thus, \hat{H} and its associated parameters are intimately related to the material

response for states within the bounding surface (i.e., for $\delta > 0$). As such, they constitute important elements of the present formulation that differentiate it from ones based on classical yield surface elastoplasticity.

3. OVERVIEW OF THE GBSM

In its most general form, the GBSM for saturated cohesive soils is a fully three-dimensional, temperature and time-dependent model that accounts for both inherent and stress induced anisotropy. To better simulate the behavior of cohesive soils exhibiting softening, the model employs a non-associative flow rule. The microfabric-inspired rotational hardening rule associated with the model was developed after a thorough review of past modeling practice. In addition, the shape hardening function used in the GBSM was developed simplifying earlier versions without compromising the model's predictive capabilities. In both cases, the selected functional form simplified earlier versions without compromising the GBSM's predictive capabilities.

3.1. Definition of Invariants.

The GBSM accounts for both inherent and stress-induced anisotropy. The mathematical representation of the latter requires the use of rotational hardening [6]. Due to the fact that the GBSM employs either an associative or non-associative flow rule, the rotation of both the plastic potential surface (PPS) and the bounding surface (BS) must be quantified. The material state is thus determined by the state of effective stress and by a suitable measure of anisotropy [7]. The rotation of both surfaces is described by the symmetric second-order anisotropic tensors α_{ij} and β_{ij} , respectively [1].

In the GBSM, *reduced* invariants of the effective stress tensor are used, thus ensuring the proper analytical treatment of anisotropic forms of the model [8]. Decomposing σ'_{ij} into

the sum of the deviatoric stress tensor s_{ij} and the hydrostatic stress gives

$$s_{ij} = \sigma'_{ij} - \frac{1}{3}\delta_{ij}\sigma'_{kk} \quad (4)$$

where δ_{ij} is the Kronecker delta. The *reduced* deviatoric stress tensors associated with the PPS and BS are thus

$$s_{ij}^{\alpha} = s_{ij} - \frac{1}{3}\alpha_{ij}\sigma'_{kk}; \quad s_{ij}^{\beta} = s_{ij} - \frac{1}{3}\beta_{ij}\sigma'_{kk} \quad (5)$$

respectively. The PPS is thus analytically described by the following invariants:

$$I = \sigma'_{ij}\delta_{ij}; \quad J^{\alpha} = \sqrt{\frac{1}{2}s_{ij}^{\alpha}s_{ij}^{\alpha}} \quad (6)$$

and

$$\theta^{\alpha} = \frac{1}{3}\sin^{-1}\left[\frac{\sqrt{3}}{2}\left(\frac{s_{ij}^{\alpha}s_{jk}^{\alpha}s_{ki}^{\alpha}}{(J^{\alpha})^3}\right)\right] \quad (7)$$

where I is the first invariant of the effective stress tensor, J^{α} is the square root of the second invariant of s_{ij}^{α} , and θ^{α} is the *reduced* Lode angle

$$(-\pi/6 \leq \theta^{\alpha} \leq \pi/6).$$

In a similar manner, the BS is analytically described by the following invariants:

$$I = \sigma'_{ij}\delta_{ij}; \quad J^{\beta} = \sqrt{\frac{1}{2}s_{ij}^{\beta}s_{ij}^{\beta}} \quad (8)$$

$$\theta^{\beta} = \frac{1}{3}\sin^{-1}\left[\frac{\sqrt{3}}{2}\left(\frac{s_{ij}^{\beta}s_{jk}^{\beta}s_{ki}^{\beta}}{(J^{\beta})^3}\right)\right] \quad (9)$$

where I is as defined in equation (6), J^{β} is the square root of the second invariant of s_{ij}^{β} , and θ^{β} is the reduced Lode angle. For θ^{α} and θ^{β} , the values of $\pm\pi/6$ correspond to conditions of

axisymmetric triaxial compression and extension, respectively.

In isotropic forms of the GBSM, both the PPS and BS are analytically defined by I , as given in equation (6) and (8), and by the following *isotropic* invariants:

$$J = \sqrt{\frac{1}{2}s_{ij}s_{ij}}; \quad \theta = \frac{1}{3}\sin^{-1}\left[\frac{\sqrt{3}}{2}\frac{s_{ij}s_{jk}s_{ki}}{(J)^3}\right] \quad (10)$$

where s_{ij} is as defined by equation (4), and $\pi/6 \leq \theta \leq \pi/6$.

In axisymmetric triaxial (p' - q) stress space, where $p' = I/3$ is the mean normal effective stress and $q = \pm\sqrt{3}J$ is the deviator stress, the measures of the anisotropic tensors α_{ij} and β_{ij} are defined by the scalar measures α and β , respectively, where

$$\alpha = \sqrt{\frac{3}{2}\alpha_{ij}\alpha_{ij}}; \quad \beta = \sqrt{\frac{3}{2}\beta_{ij}\beta_{ij}} \quad (11)$$

These quantities characterize the rotation of the PPS and the BS, respectively.

The radial mapping rule given by equation (2) is next specialized by explicitly defining a_{ij} , as well as its evolution. For monotonic loading, a_{ij} must be an isotropic tensor with a principal value on the I -axis in invariant stress space. The radial mapping rule then becomes [1]

$$\bar{I} = b(I - CI_o) + CI_o; \quad \bar{J}^{\beta} = bJ^{\beta}; \quad \bar{\theta}^{\beta} = \theta^{\beta} \quad (12)$$

where b is as previously defined, C ($0 \leq C < 1$) is the dimensionless projection center parameter, and I_o represents the point of intersection of the BS with the positive I -axis in invariant stress space (Figure 3). The inclusion of C into the formulation introduces the possibility of using a projection center $I_{PC} = CI_o$ different from the origin in stress space [9], thus allowing for the prediction of immediate negative (dilatational) pore pressure development for heavily overconsolidated samples sheared under undrained conditions. With the projection

center at the origin (i.e., for $C = 0$), the older and generally more restrictive and inaccurate formulation is retrieved [10,11], with initially positive pore pressures always being predicted, even for highly overconsolidated samples.

3.2. The Plastic Potential and Bounding Surfaces.

In its most general form, the GBSM employs a non-associative flow rule. It thus requires that a PPS be defined in addition to the BS. Both surfaces must be smooth and convex [2,3]. The most general form of the PPS associated with the GBSM is given by

$$Q(\bar{I}, \bar{J}^\alpha, \theta^\alpha, I_\alpha, \alpha) = (\bar{J}^\alpha)^2 (R - 1)^2 + \frac{\omega^2}{27} \left(\bar{I} + \frac{R - 2}{R} I_\alpha \right) (\bar{I} - I_\alpha) = 0 \quad (13)$$

where barred quantities are values of I and J^α associated with the “image” point on the PPS. The quantity I_α is the value of I at

$$\bar{J}^\alpha = \tilde{\alpha} \bar{I}, \quad \tilde{\alpha} = \alpha / (3\sqrt{3}).$$

where

The value of I_α is adjusted so that equation (13) is satisfied for the current “image” stress point (\bar{I}, \bar{J}^β) on the PPS. Kaliakin and Nieto-Leal [13] give explicit expressions for I_α associated with the various forms of the GBSM. The dimensionless model parameter R (≥ 2.0) controls the shape of the PPS [13]. Finally, ω is given by the following generalized expression:

$$\omega^2 = \frac{M - \alpha}{2} \left[2\alpha(R - 1)^2 + M - \alpha + \sqrt{4\alpha(R - 1)^2 M + (M - \alpha)^2} \right] \quad (14)$$

where the dimensionless anisotropic variable α is as previous defined in equation (11).

The quantity M is the slope of the failure surface which, in a meridional section (i.e., for a

specific value of θ^α in p' - q space, is assumed to be a straight line that coincides with the critical state line [14]. The counterpart of M in I - J^α space is

$$\tilde{M} = M / (3\sqrt{3}).$$

Both M and \tilde{M} vary with θ^α according to

$$M(\theta^\alpha, k_M) = g(\theta^\alpha, k_M) M_c$$

and

$$\tilde{M}(\theta^\alpha, k_M) = g(\theta^\alpha, k_M) \tilde{M}_c,$$

where the quantity

$$k_M = M_e / M_c = \tilde{M}_e / \tilde{M}_c,$$

with

$$M_e = M(-\pi/6) \text{ and } M_c = M(\pi/6)$$

being the values of M associated with axisymmetric triaxial extension and compression, respectively. The dimensionless function $g = g(\theta^\alpha, k_M)$ is given by [15]

$$g(\theta^\alpha, k_M) = \left[\frac{2k_M^4}{1 + k_M^4 - (1 - k_M^4) \sin 3\theta^\alpha} \right]^{\frac{1}{4}} \quad (15)$$

which has been shown to be more robust than earlier functional forms of g [1]. Figure 2 shows the variation of the PPS and failure surface with Lode angle within the octahedral plane for *anisotropic* forms of the GBSM.

The PPS given by equation (13) must satisfy two fundamental requirements. For a given value of Lode angle (θ^α), it must pass through the “image” stress point (\bar{I}, \bar{J}^β) . In addition, it must give

$$\partial Q / \partial \bar{I} = 0$$

at its intersection with the critical state (failure) line, as defined by ω ; the latter requirement is in keeping with the concept of a critical state [14].

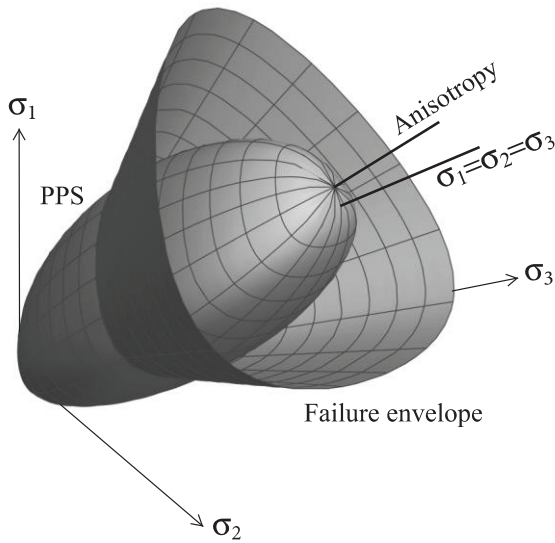


Figure 2. Plastic potential surface (PPS) and failure envelope for anisotropic form of the GBSM employing a non-associative flow rule.

Turning the attention to the definition of the BS, the results of an extensive study into suitable analytical expressions for bounding surfaces [3] showed that an elliptical form avoids potential difficulties associated with either previously used composite forms [9] or higher-order expressions. In light of this finding, the following elliptical BS is used in the GBSM model:

$$F(\bar{I}, \bar{J}^\beta, \theta^\beta, I_o, \beta) = (\bar{J}^\beta)^2 (R - 1)^2 + \frac{N^2 - \beta^2}{27} \left(\bar{I} + \frac{R - 2}{R} I_o \right) (\bar{I} - I_o) = 0 \quad (16)$$

where R is as previously defined, and barred quantities are values of I and J^β associated with the “image” point on the BS. The quantity I_o is as previously defined (Figure 3).

The parameter N defines the shape of the BS; its counterpart in stress invariant space is

$$\tilde{N} = N / (3\sqrt{3}).$$

Both N and \tilde{N} vary with θ^β according to

$$N(\theta^\alpha, k_N) = g(\theta^\alpha, k_N) N_c$$

and

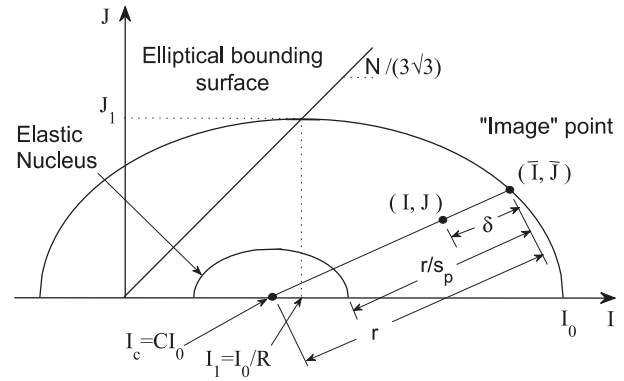


Figure 3. Schematic illustration of elliptical bounding surface and radial mapping rule in meridional section in stress invariant space for isotropic forms of the GBSM.

$$\tilde{N}(\theta^\alpha, k_N) = g(\theta^\alpha, k_N) \tilde{N}_c,$$

where the quantity

$$k_N = N_e / N_c = \tilde{N}_e / \tilde{N}_c,$$

with $N_e = N(-\pi/6)$ and $N_c = N(\pi/6)$ being the values of N associated with axisymmetric triaxial extension and compression, respectively. The dimensionless function g is given by equation (15), with θ^β and k_N replacing θ^α and k_M , respectively. Due to the fact that the GBSM is intended to be adaptive, specialization of equation (16) results in specific expressions appropriate for an associative flow rule and for the isotropic forms of the model [13].

3.3. Strain Decomposition.

The infinitesimal strain rate tensor is additively decomposed as

$$\dot{\epsilon}_{ij} = \dot{\epsilon}_{ij}^e + \dot{\epsilon}_{ij}^i = \dot{\epsilon}_{ij}^e + \dot{\epsilon}_{ij}^v + \dot{\epsilon}_{ij}^p \quad (17)$$

where the superscripts e , i , v and p denote its elastic, inelastic, viscoplastic (delayed) and plastic (instantaneous) components, respectively, and a superposed dot denotes a material time derivative or rate.

The internal variables (q_n) include proper measures of inelastic deformation that quantify the hardening of the bounding surface. An additive decomposition of \dot{q}_n into a delayed or

viscoplastic part (\dot{q}_n^v) and an instantaneous or plastic part (\dot{q}_n^p) is assumed [16]; viz.,

$$\dot{q}_n = \dot{q}_n^v + \dot{q}_n^p \quad (18)$$

Both parts are, in general, incrementally irreversible. The \dot{q}_n^v , which accounts for the delayed deformation of the cohesive soil, depends only upon the state; it can, under certain conditions, be zero. The \dot{q}_n^p , on the other hand, depends upon the state and the rates $\dot{\sigma}'_{ij}$ and \dot{q}_n^v ; it is non-zero only if the scalar loading (L) index is positive. This is done in order to emphasize the general *coupling* that exists between plastic and viscoplastic processes, whereby in addition to the $\dot{\sigma}'_{ij}$, the \dot{q}_n^v may affect the plastic loading process [17]. Since it does not enter into equation (1), the projection center tensor a_{ij} (Figure 1) is one of the internal variables. It evolves according to the rate equation

$$\dot{a}_{ij} = \dot{a}_{ij}^v + \dot{a}_{ij}^p \quad (19)$$

where a_{ij}^v and a_{ij}^p being the viscoplastic (delayed) and plastic (instantaneous) parts of a_{ij} . The elastic response is assumed to be independent of the rate of loading and to be unaltered by inelastic deformation. The elastic constitutive relations, in direct and inverse form, are

$$\dot{\epsilon}_{ij}^e = B_{ijkl} \dot{\sigma}'_{kl} \quad \text{or} \quad \dot{\sigma}'_{ij} = D_{ijkl} \dot{\epsilon}_{kl}^e \quad (20)$$

where B_{ijkl} and D_{ijkl} are the fourth-order tensors of elastic compliance and moduli, respectively. To date, bounding surface models for cohesive soils have exclusively assumed elastic isotropy. The explicit forms for B_{ijkl} and D_{ijkl} are thus typically written in terms of a non-linear elastic bulk modulus (K) and the shear modulus (G), with the latter often computed from K and a specified value of Poisson's ratio (ν). The viscoplastic response is based upon a generalization of Perzyna's elastic/viscoplastic theory [18]. The associated rate equations are

$$\dot{\epsilon}_{ij}^v = \langle \Phi \rangle R_{ij} ; \dot{q}_n^v = \langle \Phi \rangle r_n ; \dot{a}_{ij}^v = \langle \Phi \rangle r_{ij} \quad (21)$$

where R_{ij} , r_n and r_{ij} are proper tensorial functions of the state. The symbols $\langle \rangle$ again denote Macaulay brackets. In forms of the GBSM employing a non-associative flow rule, R_{ij} is the gradient of the PPS; i.e.,

$$R_{ij} = \partial Q / \partial \bar{\sigma}'_{ij}$$

If an associative flow rule is assumed, then

$$F = Q.$$

In equation (21), Φ is a continuous scalar "overstress" function. Although several explicit functional forms for $\Phi(F)$ have been proposed [13], perhaps the most commonly used form is the following "power" form:

$$\Phi = \frac{1}{V} (\Delta \hat{\sigma})^n = \frac{1}{V} \left[\frac{\hat{\delta}}{r \left(1 - \frac{1}{s_v} \right)} \right]^n \quad (22)$$

where n and V are positive model parameters, and $\Delta \hat{\sigma}$ is a "normalized overstress" [16]. In equation (22) r is as defined in Figure 1, $s_v (> 1)$ is a dimensionless model parameter, and $\hat{\delta}$ is the Euclidean distance between σ'_{ij} and a second "image" stress $\hat{\sigma}'_{ij}$ on the boundary of a second elastic nucleus that is associated with the viscoplastic response and is homologous with the bounding surface. This elastic nucleus assumes the role of the "static" yield surface proposed by Perzyna [18]. Since the material is assumed to be inviscid in the elastic region, $\dot{\epsilon}_{ij}^v$ becomes zero when $\Delta \hat{\sigma} \leq 0$; i.e., when σ'_{ij} is either on or within the second elastic nucleus. The definition of the plastic response is predicated on *four* expressions associated with the bounding surface concept. First, the BS defines the direction of inelastic loading-unloading (L_{ij}). In particular, the expression for

L_{ij} at the actual stress point (σ'_{ij}) is defined as the gradient of F at the “image” point (Figure 1); viz.,

$$L_{ij} \equiv \nabla F = \partial F / \partial \bar{\sigma}'_{ij}.$$

Secondly, a scalar loading index (L) must be defined in terms of L_{ij} , the rate of the effective stress tensor, and the plastic moduli K_p ; viz. [17],

$$L = \frac{1}{K_p} \left[L_{ij} \dot{\sigma}'_{ij} + \langle \Phi \rangle \frac{1}{b} \frac{\partial F}{\partial q_n} r_n - \langle \Phi \rangle \left(1 - \frac{1}{b} \right) \frac{\partial F}{\partial \bar{\sigma}'_{ij}} r_{ij} \right] \quad (23)$$

where L_{ij} and the dimensionless parameter b are as previously defined, and K_p is given by equation (3), which constitutes the third of the aforementioned expressions associated with the bounding surface concept. The presence of r_n and r_{ij} in equation (23) shows that L couples the plastic-viscoplastic hardening response for states on and within the bounding surface. Additional details pertaining to the terms appearing in this equation are given elsewhere [13,16].

When the stress point lies on the bounding surface, $\delta = 0$ (Figure 1),

$$K_p = \bar{K}_p, \quad \dot{\sigma}'_{ij} = \dot{\bar{\sigma}}'_{ij}$$

and equation (23) simplifies accordingly. As noted in conjunction with equation (3), an explicit expression for \bar{K}_p , which is the fourth expression associated with the bounding surface concept, is determined from the consistency condition $\dot{F} = 0$. Additional details pertaining to the determination of \bar{K}_p are given elsewhere [13].

The rate equations for plastic response are given by

$$\dot{\varepsilon}_{ij}^p = \langle L \rangle R_{ij}; \quad \dot{q}_n^p = \langle L \rangle r_n; \quad \dot{a}_{ij}^p = \langle L \rangle r_{ij} \quad (24)$$

where R_{ij} , r_n , and r_{ij} are as previously defined.

3.4. Hardening Rules.

In all forms of the GBSM, the BS hardens isotropically along the I -axis. The proper simulation of stress-induced anisotropy for anisotropic forms of the GBSM also requires that the BS and PPS undergo rotational hardening (RH) [7].

The isotropic hardening is controlled by a single scalar internal variable that measures the increment in inelastic volumetric strain; viz.,

$$\dot{\varepsilon}_{kk}^i = \dot{\varepsilon}_{kk}^v + \dot{\varepsilon}_{kk}^p = (\langle \Phi \rangle + \langle L \rangle) R_{kk} \quad (25)$$

where $R_{kk} = \partial Q / \partial \bar{I}$.

It is convenient to relate the evolution of the BS to the increment in inelastic volumetric strain through the value of I_o (recall Figure 3). The resulting analytical expression describing the isotropic hardening is [9,13]

$$\dot{I}_o = \frac{1 + e_{in}}{\lambda - \kappa} (\langle I_o - I_L \rangle + I_L) \dot{\varepsilon}_{kk}^i \quad (26)$$

where the critical state parameters λ and κ are equal to the negative of the slopes of the virgin consolidation and swell/recompression lines, respectively, in a plot of void ratio (e) versus the natural logarithm of I [14], and e_{in} represents the initial total void ratio corresponding to the reference configuration with respect to which engineering strains are measured; for natural strains, it represents the current total void ratio. The nonzero limiting “transitional” stress I_L is included in equation (26) so that for $I < I_L$ the relation between I and the elastic part of the void ratio (e^e) changes continuously from logarithmic to linear [9]. The singularity of the elastic stiffness near $I = 0$, resulting from excessive material softening, is thus removed. The quantity I_L is *not* a model parameter; its value is typically taken equal to one-third of the atmospheric pressure (P_a) [1].

The evolution of the stress-induced anisotropy during shearing is mathematically accounted for by RH of the BS (through the anisotropic tensor b_{ij}) and, if applicable, the PPS (through the anisotropic tensor a_{ij}). Recently [19], robust RH

rules for the BS and PPS, that were inspired by earlier formulations and by experimental observations of microfabric evolution of cohesive soils, were proposed. Nieto-Leal et al. [19] give additional details pertaining to these RH rules.

3.5. The Shape Hardening Function.

The positive hardening function \hat{H} defines the shape of the response curves during inelastic hardening (or softening) for points *within* the BS [2]. It relates the plastic modulus K_p to its “bounding” value in the manner given by equation (3). For the GBSM,

$$\hat{H} = \frac{(1 + e_{in})}{\lambda - \kappa} P_a \left[9 (F, \bar{I})^2 + \frac{1}{3} (F, \bar{J}^\beta)^2 \right] [h(\theta^\beta) z^{0.02} + h_o (1 - z^{0.02})] f_n \quad (27)$$

where e_{in} , λ , κ , and P_a are as previously defined. For brevity, the partial derivative with respect to an invariant is denoted with a comma followed by the symbol of the invariant as a subscript. The definition of the dimensionless variable z varies depending on the form of the GBSM used. For, example, for the *anisotropic* form of the GBSM employing a *non-associative* flow rule, z is given by

$$z = J^\beta / J_1^\beta = J^\beta / (\tilde{N} I_1) = 3\sqrt{3} J^\beta R / N I_o$$

(see Figure 3).

The dimensionless quantity $h(\theta^\beta)$ in equation (27) has the general form $h(\theta^\beta) = g(\theta^\beta, k_h) h_c$, where $k_h = h_e/h_c$, with $h_e = h(-\pi/6)$ and $h_c = h(\pi/6)$ being the values of h associated with axisymmetric triaxial extension and compression, respectively. The dimensionless function g is given by equation (15), with θ^β and k_h replacing θ^α and k_M , respectively.

Finally, the expression for f_n appearing in equation (27) is a generalization of the form given by Nieto-Leal and Kaliakin [5]; viz.,

$$f_n = \frac{1}{2} \left[a + \text{sign}(n_I) (|n_I|)^{\frac{1}{5}} \right] \left(\frac{I}{I_o} \right) \quad (28)$$

where a (> 1.0) is a dimensionless model parameter [13], and n_I is the component, in the \bar{I} direction, of the unit outward normal to the bounding surface in stress invariant space. For the *anisotropic* form of the GBSM with a *non-associative* flow rule,

$$n_I = \frac{F, \bar{I}}{\sqrt{(F, \bar{I})^2 + (F, \bar{J}^\beta)^2}} \quad (29)$$

If an associative flow rule is used instead, F, \bar{J}^β is replaced by F, \bar{J}^α in equations (27) and (29) and in the definition for z . Finally, if an isotropic form of the GBSM is used, F, \bar{J}^β is replaced by F, \bar{J} in the aforementioned equations.

4. THE INITIAL MATERIAL STATE

The definition of the initial state for all forms of the GBSM requires knowledge of the initial value (e_{in}) of the void ratio, which is one of the internal variables. In addition, the initial stress state is defined in terms of values of the total confining stresses, the total stresses associated with the maximum past preconsolidation pressure, and the initial excess pore fluid pressure.

Anisotropic forms of the GBSM require the specification of the inherent anisotropy. This is achieved by specifying the initial values of the anisotropic tensor, which is another type of internal variable. These values are commonly determined from the results of laboratory tests on anisotropically consolidated specimens. For the special case of a transversely anisotropic (or “cross-anisotropic”) soil in which the x_1 direction is taken normal to the plane of isotropy, $\sigma'_2 = \sigma'_3$. For this case, the stress ratio ($\eta = q/p'$) in axisymmetric triaxial space is given by

$$\eta_{K_c} = 3(1 - K_c)/(1 + 2K_c),$$

where $K_c = \sigma'_3/\sigma'_1$

is the effective stress ratio. Recalling the definition of the scalar representation (α) of α_{ij}

in axisymmetric triaxial space given by equation (11), it is relatively well established [20] that the value of α determined using an anisotropic constitutive model will be *less* than η . Thus,

$$\eta = \alpha/A, \text{ where } A \leq 1.0.$$

For transversely anisotropic soils, the inherent (initial) values of α_{ij} are thus given by

$$\alpha_{11}^{in} = \frac{2A(1 - K_{in})}{1 + 2K_{in}}; \alpha_{22}^{in} = \alpha_{33}^{in} = -\frac{1}{2}\alpha_{11}^{in} \quad (30)$$

with

$$\alpha_{12}^{in} = \alpha_{21}^{in} = \alpha_{13}^{in} = \alpha_{31}^{in} = \alpha_{23}^{in} = \alpha_{32}^{in} = 0.$$

Here K_{in} denotes the constant initial effective stress ratio to which a soil has been subjected in a drained axisymmetric triaxial (isotropic) or oedometer (anisotropic) test.

In the anisotropic form of the GBSM employing a non-associative flow rule, α_{ij} represents the rotation of the PPS. The rotation of the BS is quantified through the symmetric anisotropic tensor β_{ij} . The measure of this tensor in axisymmetric triaxial stress space is defined by the scalar β , given by equation (11). Since the value of β associated with loading at a prescribed stress ratio η is purported to be equal to this ratio [20], the initial values of β_{ij} , corresponding to a transversely anisotropic stress, will be

$$\beta_{11}^{in} = \frac{2(1 - K_{in})}{1 + 2K_{in}}; \beta_{22}^{in} = \beta_{33}^{in} = -\frac{1}{2}\beta_{11}^{in} \quad (31)$$

with $\beta_{12}^{in} = \beta_{21}^{in} = \beta_{13}^{in} = \beta_{31}^{in} = \beta_{23}^{in} = \beta_{32}^{in} = 0$.

where K_{in} is as previously defined. The initial values of α_{ij} is again given by equation (30).

5. THE MODEL PARAMETERS

Since the GBSM includes both isotropic and anisotropic formulations, together with both

associative and non-associative flow rules, the number of parameter values to be determined depends on the specific form of the model that is being used. To facilitate the subsequent discussion, the anisotropic forms of the GBSM employing non-associative and associative flow rules are referred to as GBSMan and GBSMaa, respectively; the isotropic forms of the model employing non-associative and associative flow rules are referred to as GBSMin and GBSMia, respectively.

The model parameters associated with all forms of the GBSM are grouped by their type as follows: The critical state parameters λ , κ , M_c and M_e ; the elastic parameters G or ν ; the surface configuration parameters R , N_c , and N_e , the projection center parameter C ; the elastic nucleus parameter s_p ; the shape hardening parameters h_c , h_e , and a ; the rotational hardening parameters χ_η , ψ_1 , and ψ_2 , and the viscoplastic parameters s_v , V , and n . All of the above parameters are *positive*; with the exception of G and V , all parameters are dimensionless. Table 1 summarizes the model parameters associated with the *most general* forms of each of the forms of the GBSM.

With the exception of the viscoplastic parameters s_v , V , and n , values for all other (elastoplastic) parameters are determined from results of standard laboratory tests of short enough duration to ensure that time and rate effects are negligible. With some exceptions, the elastoplastic model parameters are identical to those used in conjunction with previous rate independent bounding surface formulations.

Most of the model parameter values are determined by curve-fitting; the availability of high-quality experimental data is thus requisite for obtaining accurate parameter calibrations. Although it would perhaps be desirable to determine the model parameter values from closed-form formulas, such expressions are rarely available. Even when such expressions exist, the results they give are not always reliable. Thus, although curve fitting may be viewed as being somewhat simple-minded, with the proper guidelines it gives a safe and intuitive way in

which to determine values for the model parameters. The values typically selected for the model parameters either are fixed for most soils, or fall within fairly narrow ranges. Furthermore, the values of some of these parameters can be determined from standard soil test parameters.

Table 1. Parameters Associated with the GBSM.

GBSM _{an}	GBSM _{aa}	GBSM _{in}	GBSM _{ia}
λ	λ	λ	λ
κ	κ	κ	κ
M_c	M_c	M_c	M_c
M_e	M_e	M_e	M_e
G or ν	G or ν	G or ν	G or ν
R	R	R	R
N_c	-	N_c	-
N_e	-	N_e	-
C	C	C	C
s_p	s_p	s_p	s_p
h_c	h_c	h_c	h_c
h_e	h_e	h_e	h_e
a	a	a	a
χ_η	χ_η	χ_η	χ_η
ψ_1	ψ_1	-	-
ψ_2	ψ_2	-	-
s_v	s_v	s_v	s_v
V	V	V	V
n	n	n	n

To establish the values of the necessary parameters associated with the *most general* form of the GBSM, a minimum of *eight* laboratory tests are required, namely: (a) A single isotropic or anisotropic (one-dimensional) consolidation or drained compression test with both loading and unloading phases, (b) Consolidated-undrained (preferable) or drained axisymmetric triaxial compression and extension tests (with pore pressure measurements) on anisotropically or isotropically consolidated specimens in the normally, lightly, and heavily overconsolidated regions (a total of six tests), and (c) At least one long term test such as undrained or drained triaxial creep or stress relaxation.

If a less general form of the bounding surface model is acceptable, both the number of model parameters involved and the number of laboratory tests required can be significantly reduced. For example, if only time independent analyses are to be considered, values of the three viscoplastic model parameters, as well as the long-term experiment(s) used in their determination, are no longer required. Furthermore, if the model is only to be used for the time-independent analysis of isotropically consolidated normally consolidated soils loaded in triaxial compression or extension, the number of required model parameters reduces to five, and only data from a consolidation test and a single triaxial test are required for the model calibration. Similar reductions in the number of required model parameters can be realized for overconsolidated soils by neglecting the difference between hardening parameters in compression and extension.

6. ASSESSMENT OF PERFORMANCE

To assess the simulative and predictive capabilities of the GBSM and to illustrate its flexibility, four soils were simulated using the model. All of the simulations and predictions shown in this section were generated using the CALBR8 computer program [21].

The simulative capabilities of the *simplest* (GBSM_{ia}) form of the GBSM, as applied to isotropically consolidated undrained compression (CIUC) test experimental results for normally consolidated Bangkok clay, were recently assessed [1]. Even though only five model parameters λ , κ , M_c , ν , and R are active in such applications, the agreement between GBSM_{ia} simulations and experimental results was excellent.

6.1 Simulation of Taipei Silty Clay.

In light of the aforementioned simulation effort, the ability of the GBSM to simulate the more complex anisotropic, softening response is thus first assessed herein. Since the proper

simulation of softening requires the use of a non-associative flow rule [20], the present simulations require the use of the most complex form of the model; i.e., the anisotropic non-associative version (GBSMan).

The soil considered is Taipei silty clay (TSC). The data set used in the present assessment of the GBSMan form of the model was generated by Chin and Liu [22], who performed a set of axisymmetric triaxial CK_0UC and CK_0UE tests on samples with OCRs of 1.0, 2.0, and 4.0. The TSC tested had a liquid limit (w_L) of 40% and a plasticity index (I_p) of 22%.

The following values for the critical state parameters were obtained directly from the data of Chin and Liu [22]: $\lambda = 0.17$, $\kappa = 0.02$, $M_c = 1.05$, and $M_e = 0.95$. The Poisson's ratio equal to 0.29 was assumed. A value of $R = 2.50$ was determined by matching the experimental undrained stress paths for the normally consolidated samples. A value of 0.65 for the projection center parameter (C) was determined from a best fit of the undrained stress paths for OCRs of 2.0 and 4.0. Values for the shape hardening parameters $h_c = 5.0$, $h_e = 25.0$, and $a = 1.5$ were determined from a best fit of the deviator stress versus axial strain response for these same OCR values. A value of 1.0 for the elastic nucleus parameter s_p , which reduces the nucleus to a point, was found to be adequate. Values of the configuration parameters N_c and N_e equal to 0.90 and 1.13, respectively, were determined by matching the response in compression and extension for the normally consolidated sample. Finally, the rotational hardening parameters were assigned values of $\chi_\eta = 1.5$, $\psi_1 = 200.0$ and $\psi_2 = 50.0$.

The time-independent model simulations were obtained using the aforementioned parameter values. Figure 4 compares the simulations of anisotropically consolidated samples with experimental values. From this figure, it is evident that the agreement between the simulated and experimental normalized undrained stress paths is quite good. The normalized deviator stress versus axial strain simulations are somewhat less accurate than the

undrained stress paths. Chin and Liu [22] did not report any experimental values for excess pore pressure.

6.2. Simulation of Grundite Clay.

Since the GBSM is formulated in terms of three stress invariants, its predictive capabilities under true triaxial (TT) states of stress are next investigated. In TT tests, the values of the three principal stresses can be varied independently. The relative magnitude of the intermediate principal stress (σ_2) is typically expressed by means of the following ratio between principal stress differences: $b_{TT} = (\sigma_2 - \sigma_3)/(\sigma_1 - \sigma_3)$, where it is assumed that $\sigma_1 \geq \sigma_2 \geq \sigma_3$. The ratio b_{TT} is zero (0.0) for axisymmetric triaxial compression, where $\sigma_2 = \sigma_3$; it is equal to unity (1.0) for axisymmetric triaxial extension, where $\sigma_1 = \sigma_2$. Based on the results of past TT tests [23-30], the relative magnitude of the intermediate principal stress has a significant influence on the three-dimensional stress-strain, strength, and volume change or pore pressure characteristics of cohesive soils.

Lade and Musante [25] experimentally studied the influence of the intermediate principal stress on the stress-strain, pore pressure and strength characteristics of a remolded clay under undrained conditions. In this study, consolidated-undrained axisymmetric triaxial compression tests and TT tests with independent control of all three principal stresses on cubical specimens were performed.

The soil used in all tests performed by Lade and Musante [25] was called "Grundite" clay, which is a trade name used by the Illinois Clay Products Company. Grundite is composed primarily of the clay mineral illite, and is mined in the Goose Lake area of Illinois [31]. The particle size distribution indicated that the clay consisted of about equal amounts of silt and clay size particles. The w_L and I_p of the soil were equal to 54.8% and 30.1%, respectively. Lade and Musante did not report the specific gravity of solids (G_s) for Grundite clay.

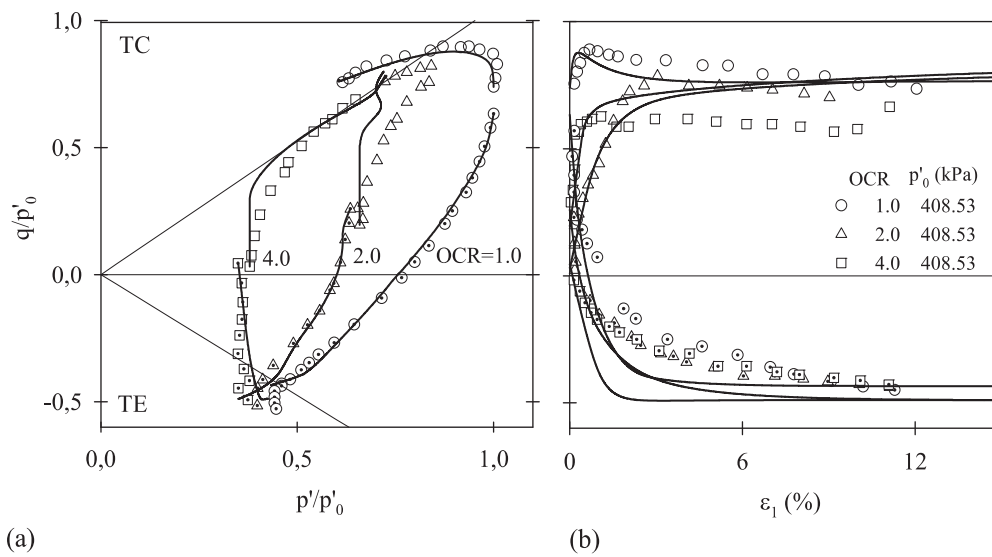


Figure 4. Comparison of simulated and experimental undrained response of anisotropically consolidated samples of TSC for data of Chin and Liu [22].

However, in their experimental study of the same soil, Perloff and Osterberg [32] and Kondner and Horner [33] reported a value of G_s equal to 2.74 (they also reported w_L and I_P values equal to 54.5% and 28.5%, respectively, which are very close to the values reported by Lade and Musante). Consequently, a value of G_s equal to 2.74 was used to compute initial values of void ratio (described below) for all numerical simulations reported herein.

All specimens of Grundite clay used in Lade and Musante's study were produced from a slurry with a water content of 90%. The uniform slurry was consolidated in a double draining consolidometer at a vertical pressure smaller than the final isotropic consolidation pressure to be used in the subsequent tests. After consolidation, specimens were thoroughly remolded to eliminate the inherent anisotropy due to the initial K_0 consolidation. Specimens with the respective shapes were next trimmed, installed in the testing apparatus, and consolidated isotropically at 98.0 kPa, 147.0 kPa, and 196.0 kPa, corresponding to water contents of 34.4, 31.9 and 30.1%, respectively. For a value of G_s equal to 2.74, the associated values of initial void ratio (e_{in}) are 0.943, 0.874 and 0.825. With the exception of triaxial compression, Lade and Musante [25] presented

experimental results only for a confining stress of 147.0 kPa.

Following the above preliminary tests, three series of consolidated-undrained tests were performed in a cubical triaxial apparatus similar to that described by Lade and Duncan [34]. This apparatus was designed to permit application of three unequal principal stresses to a cubical specimen. The side dimensions of the specimen were 76 mm. Each test in the series was conducted with constant confining pressure σ_3 . The horizontal and vertical deviator stresses were increased proportionally until the specimen failed. The ratio: b_{TT} between the deviator stresses was maintained constant in each test. For each consolidation pressure, the values of: b_{TT} used in the tests were chosen so that the failure surface, the stress-strain relations, and the pore pressure response could be determined over the full range of the intermediate principal stress. Lade and Musante [25] noted that the response of specimens of remolded Grundite clay was essentially isotropic. The strengths of test specimens with b_{TT} values equal to 0.95 (i.e., near triaxial extension) were approximately the same whether they failed horizontally or vertically. Lade and Musante [25] did not show consolidation data for Grundite clay. However,

based on laboratory data [35] for two isotropic compression tests and one K_0 consolidation test performed on Grundite clay, an average value of λ equal to 0.152 was determined. Since no rebound data was available, the aforementioned work of Perloff and Osterberg [32] and Kondner and Horner [33] was consulted. Perloff and Osterberg [32] performed isotropic compression tests with loading and rebound phases on 23 specimens of Grundite clay. The average values of λ and κ associated with these tests were 0.152 and 0.076, respectively. Consequently, these values were used in the present simulations of Grundite clay.

The determination of the slope of the critical state line in triaxial compression (M_c) and extension (M_e) requires the values of the effective friction angle for both states. In the case of triaxial compression ($b_{TT} = 0.0$) of cubical samples, Lade and Musante [25] computed effective friction angles ϕ'_c of 30.6, 28.2 and 27.4° for consolidation stresses of 98.0 kPa, 147.0 kPa, and 196.0 kPa, respectively. In axisymmetric triaxial tests performed on the same soil [35], ϕ'_c values equal to 29.6, 30.1 and 30.1° were computed for tests with a consolidation stress of 98.0 kPa. In two tests with a consolidation stress of 147.0 kPa, ϕ'_c values of 29.3 and 28.7° were computed. Finally, in two tests with a consolidation stress of 196.0 kPa, ϕ'_c values of 27.9 and 28.2° were computed. The overall average of these values is 29.1°. Using this friction angle gives

$$M_c = \frac{6 \sin \phi'_c}{3 - \sin \phi'_c} = 1.163 \quad (32)$$

In two true triaxial tests near extension ($b_{TT} = 0.95$), Lade and Musante [25] obtained effective friction angles of 30.6 and 31.2° for a consolidation stress of 147.0 kPa. The results of additional true triaxial tests at consolidation stresses of 98.0 kPa and 196.0 kPa yielded ϕ'_e values of 35.1 and 31.0°, respectively. The overall average of these values is 31.0°. Using this friction angle gives

$$M_e = \frac{6 \sin \phi'_e}{3 + \sin \phi'_e} = 0.900 \quad (33)$$

The ratio M_e/M_c is thus equal to 0.774. For the similar illitic clay tested by France and Sangrey [36] this ratio was equal to 0.76.

A value of Poisson's ratio ν equal to 0.27 was assumed. This is consistent with the empirical relation presented by Lade [37] for an I_p of approximately 30%.

Since the Grundite clay specimens were purported to be normally consolidated, the bounding surface shape parameter R would normally be determined from the three undrained triaxial compression tests (i.e., for $b_{TT} = 0.00$) at consolidation stresses of 98.0 kPa, 147.0 kPa, and 196.0 kPa. However, a plot of the associated undrained stress paths showed that these more closely resembled ones for lightly overconsolidated specimens. While this is likely due to the fact that the soil was repeatedly remolded, it nonetheless requires that these tests be modeled as slightly overconsolidated. As such, the overconsolidation ratio was numerically estimated to be approximately 1.5. This ratio was maintained in all of the numerical simulations of Grundite clay. Since the specimens are lightly overconsolidated, the magnitude of the projection center parameter C influences the simulations. From the shape of the undrained stress paths for the three tests at $b_{TT} = 0.00$, it was determined that a value of C equal to 0.20 was appropriate.

A value for the shape hardening parameter associated with triaxial compression (h_c) was determined by best matching the experimental results for $b_{TT} = 0.21$ and 0.40. The value for the shape hardening parameter associated with triaxial compression (h_e) was determined by matching the experimental results for $b_{TT} = 0.95$. As in the case of many other soils, the remaining shape hardening parameter (a) was taken equal to 1.2. Finally, values of the configuration parameters N_c and N_e equal to 1.125 and 0.870, respectively, were determined

by matching the experimental results for $b_{TT} = 0.00$ and 0.95 .

Using the aforementioned parameter values in conjunction with the GBSMin form of the GBSM, the TT tests performed by Lade and Musante [25] were simulated numerically. Following the actual experimental procedure, in each simulation the minor principal total stress (σ_3) was maintained constant. The major and intermediate total stress were increased in such a manner so as to maintain the experimental values of b_{TT} (i.e., 0.00, 0.21, 0.40, 0.70, and 0.95) constant. Figures 5 to 8 summarize the results of these time-independent simulations and compare them to the experimental results. In these figures, experimental results are depicted by discrete symbols. The simulated results are depicted by continuous curves; in the legends these results are denoted by the “(sim)”. Figure 5 compares the simulated principal effective stress difference ($\sigma'_1 - \sigma'_3$) versus major principal strain (ϵ_1) response with

experimental values. Although the experimental results for $b_{TT} = 0.40$ are somewhat under predicted, the overall agreement between simulated and experimental results is quite good.

Figure 6 compares the simulated excess pore pressure versus ϵ_1 response with experimental values. Although the ϵ_1 response for $b_{TT} = 0.21$ is under predicted, the overall agreement between simulated and experimental results is quite good.

In Figures 7 and 8 are shown the comparisons between the simulated and experimental principal strain response. From Figure 7 it is evident that the simulated ϵ_2 versus ϵ_1 response is somewhat under predicted for $b_{TT} = 0.21$. The agreement between the simulated and experimental response for the other values of b_{TT} is, however, much better. Similar conclusions are drawn in the case of the major (ϵ_1) versus minor principal strain (ϵ_3) response (Figure 8).

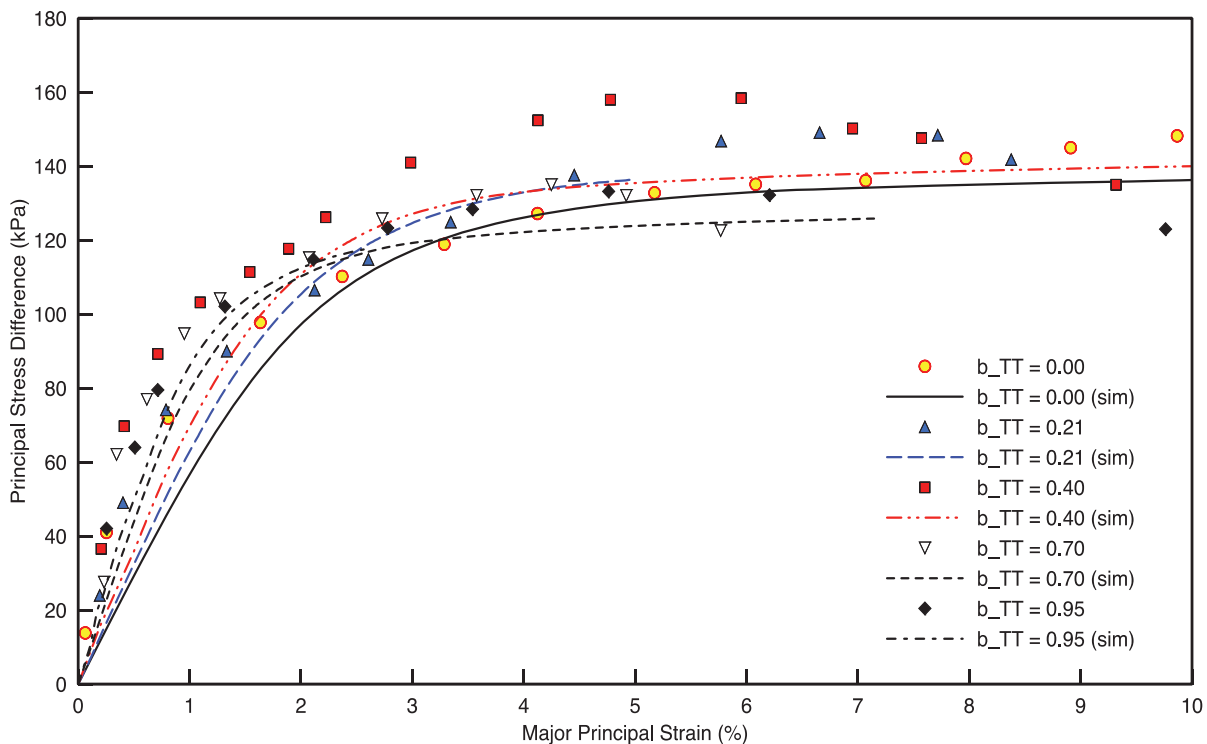


Figure 5. Comparison of simulated and experimental principal stress difference vs. major principal strain response of TT tests on samples of undrained Grundite clay [37].

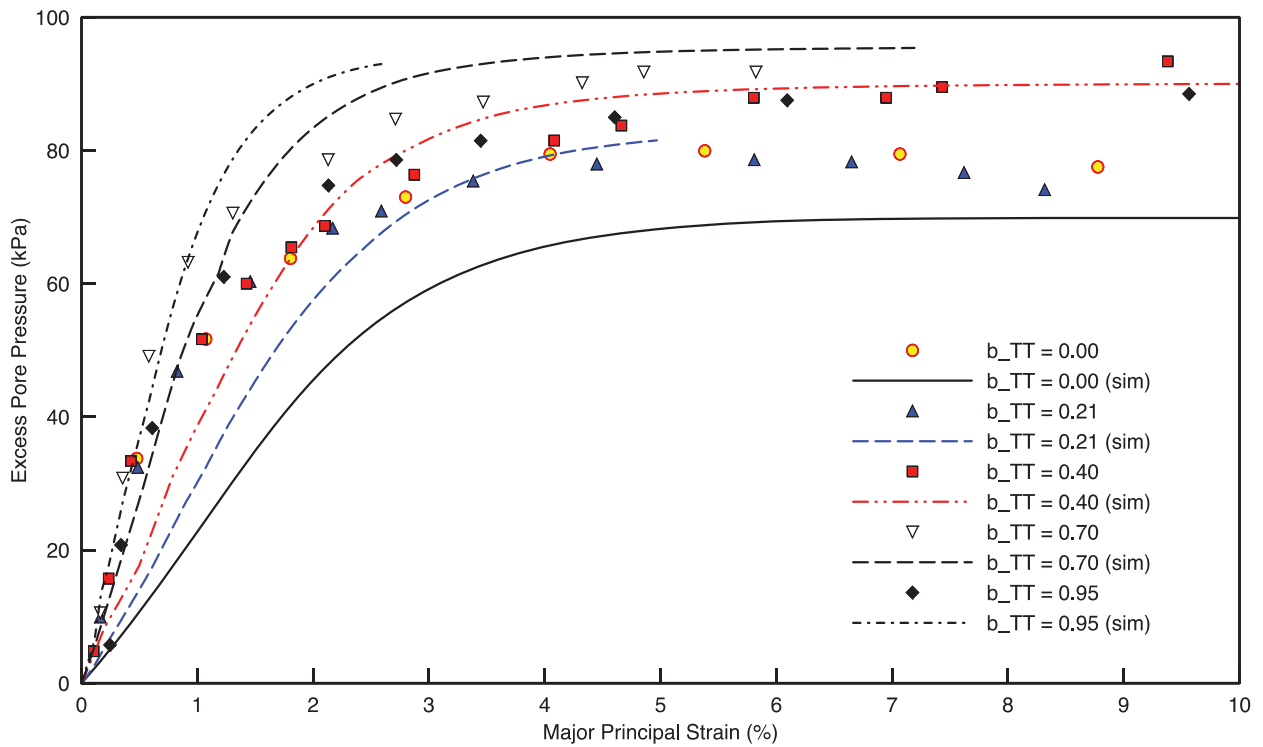


Figure 6. Comparison of simulated and experimental excess pore pressure vs. major principal strain response of TT tests on samples of undrained Grundite clay [37].

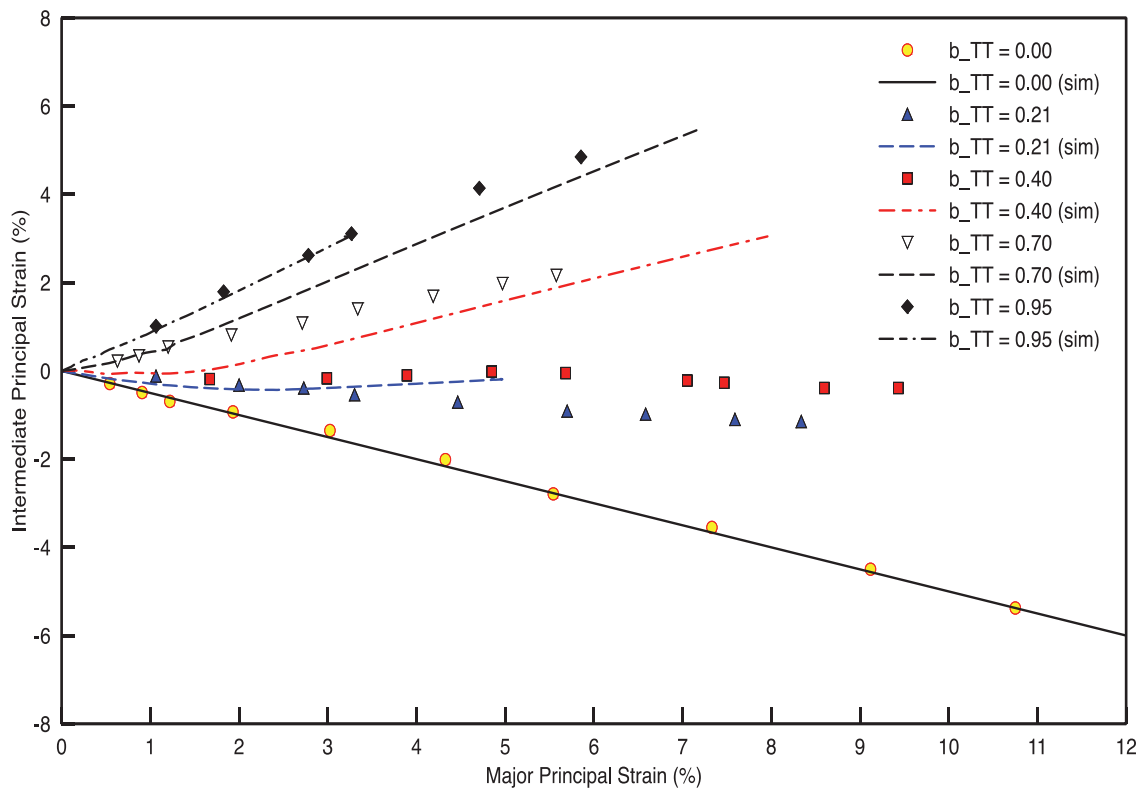


Figure 7. Comparison of simulated and experimental intermediate vs. major principal strain response of TT tests on samples of undrained Grundite clay [37].

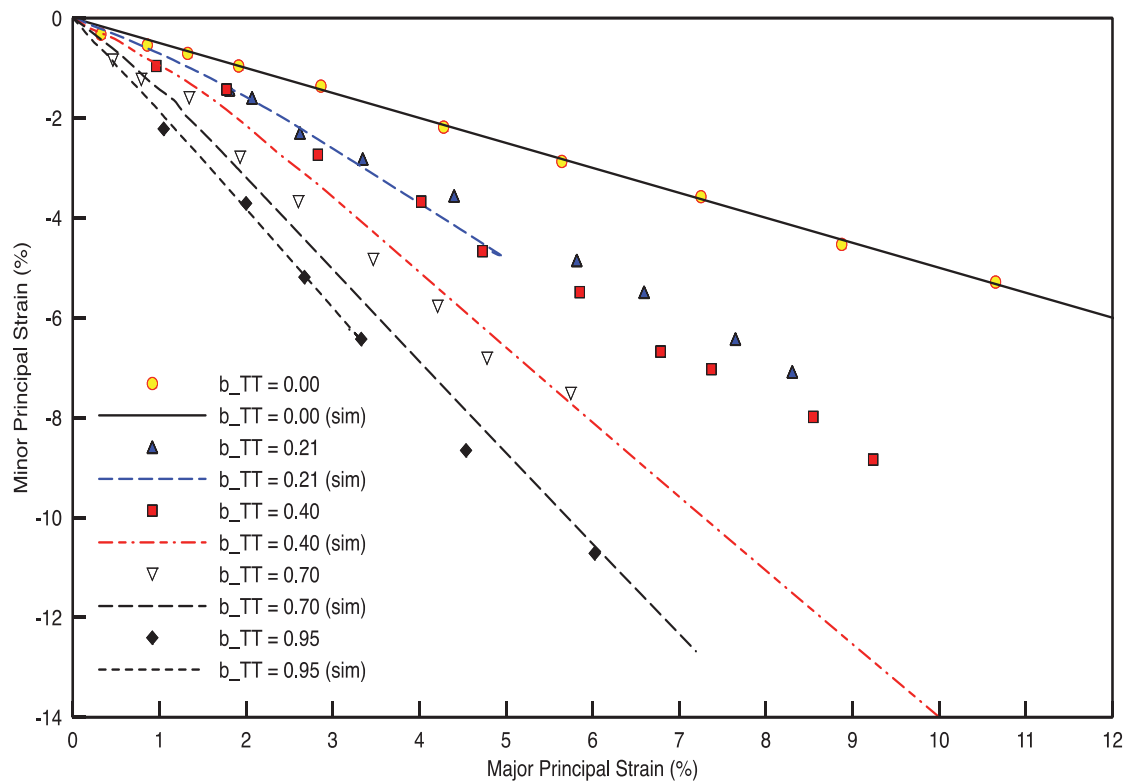


Figure 8. Comparison of simulated and experimental minor vs. major principal strain response of TT tests on samples of undrained Grundite clay [37].

7. CONCLUSIONS

The Generalized Bounding Surface Model (GBSM) synthesizes many previous forms of the bounding surface model for cohesive soils and improves upon many aspects of these models. The GBSM is a fully three-dimensional, time-dependent model that accounts for both inherent and stress induced anisotropy through a suitable rotational hardening laws. In addition, the model employs either an associative or non-associative flow rule. This paper assessed the model's performance in simulating the response of *soft*, saturated cohesive soils. Based on comparisons with experimental results for two different saturated cohesive soils, the GBSMan and GBSMin forms of the GBSM were shown to realistically simulate the time-independent, isothermal response of such soils when subjected to monotonic loading.

REFERENCES

1. **Kaliakin V.N., Leal A.N., Mashayekhi M.** Modeling the Time- and Temperature-Dependent Response of Cohesive Soils in a Generalized Bounding Surface Framework. // *Transportation Infrastructure Geotechnology*, 2018, Vol. 5, No. 3, pp. 250-286.
2. **Dafalias Y.F.** Bounding Surface Plasticity. I: Mathematical Foundation and the Concept of Hypoplasticity. // *Journal of Engineering Mechanics*, ASCE, Vol. 112, No. 90, 1986, pp. 966-987.
3. **Nieto-Leal A., Kaliakin V.N.** On Soil Yielding and Suitable Choices for Yield and Bounding Surfaces. Report, Department of Civil and Environmental Engineering, University of Delaware, DE, 2013.
4. **Dafalias Y.F.** The Concept and Application of the Bounding Surface in Plasticity Theory. // *IUTAM Symposium on Physical Non-Linearities in Structural Analysis*, Hult

- J. and Lemaitre J. (Eds.). Springer-Verlag, Berlin, 1981, pp. 56-63.
5. **Nieto-Leal A., Kaliakin V.N.** Improved Shape Hardening Function for Bounding Surface Model for Cohesive Soils // *Journal of Rock Mechanics and Geotechnical Engineering*, 2014, Vol. 6. No. 3, pp. 327-337.
 6. **Dafalias Y.F.** An Anisotropic Critical State Soil Plasticity Model. // *Mechanics Research Communications*, 1986, Vol. 13, No. 6, pp. 341-347.
 7. **Baker R., Desai C.S.** Induced Anisotropy During Plastic Straining. // *International Journal for Numerical and Analytical Methods in Geomechanics*, 1984, Vol. 8, No. 2, pp. 167-185.
 8. **Crouch R.S., Wolf J.P.** On a Three-dimensional Anisotropic Plastic Model for Soil. // *Geotechnique*, 1995, Vol. 45, No. 2, pp. 301-305.
 9. **Dafalias Y.F., Herrmann L.R.** Bounding Surface Plasticity II: Application to Isotropic Cohesive Soils. // *Journal of Engineering Mechanics*, ASCE, 1986, Vol. 112, No. 12, pp. 1263-1291.
 10. **Dafalias Y.F., Herrmann L.R.** A Bounding Surface Soil Plasticity Model. // *Proceedings of the International Symposium on Soils Under Cyclic and Transient Loading*, Pande G.N. and Zienkiewicz O.C. (Eds.), A.A. Balkema, Rotterdam, 1980, pp. 335-345.
 11. **Dafalias Y.F., Herrmann L.R.** Bounding Surface Formulation of Soil Plasticity. // *Soil Mechanics – Transient and Cyclic Loads*, Pande G.N. and Zienkiewicz O.C. (Eds.), John Wiley and Sons, Chichester, UK, Chapter 10, 1982, pp. 253-282.
 12. **Kaliakin V.N., Nieto-Leal A.** Details Pertaining to the Generalized Bounding Surface Model for Cohesive Soils. Revised & Expanded, Report, Department of Civil and Environmental Engineering, University of Delaware, DE, 2017.
 13. **Kaliakin V.N., Dafalias Y.F.** Simplifications to the Bounding Surface Model for Cohesive Soils. // *International Journal for Numerical and Analytical Methods in Geomechanics*, 1989, Vol. 13, No. 1, pp. 91-100.
 14. **Schofield A.N., Wroth C.P.** Critical State Soil Mechanics. McGraw-Hill Book Co., Inc., London, UK, 1968, 310 pages.
 15. **Sheng D., Sloan S.W., Yu H.S.** Aspects of finite element implementation of critical state models. // *Computational Mechanics*, 2000, Vol. 26, pp. 185-196.
 16. **Kaliakin V.N., Dafalias Y.F.** Theoretical Aspects of the Elastoplastic-Viscoplastic Bounding Surface Model for Cohesive Soils. // *Soils and Foundations*, 1990, Vol. 30, No. 3, pp. 11-14.
 17. **Dafalias Y.F.** Bounding Surface Elastoplasticity-Viscoplasticity for Particulate Cohesive Media. // *Deformation and Failure of Granular Materials, IUTAM Symposium on Deformation and Failure of Granular Materials*, Vermeer P.A. and Luger H.J. (Eds.), A.A. Balkema, Rotterdam, 1982, pp. 97-107.
 18. **Perzyna P.** Fundamental Problems in Viscoplasticity. // *Advances in Applied Mechanics*, 1966, Vol. 9, pp. 243-377.
 19. **Nieto-Leal A.N., Kaliakin V.N., Mashayekhi M.** Improved RH rule for cohesive soils and inherent anisotropy. // *International Journal for Numerical and Analytical Methods in Geomechanics*, 2018, Vol. 42, No. 3, pp. 469-487.
 20. **Dafalias Y.F., Manzari M.T., Papadimitriou A.G.** SANICLAY: simple anisotropic clay plasticity model. // *International Journal for Numerical and Analytical Methods in Geomechanics*, 2006, Vol. 30, No. 12, pp. 1231-1257.
 21. **Kaliakin V.N.** CALBR8, A Simple Computer Program for Assessing the Idiosyncrasies of Various Constitutive Models Used to Characterize Soils. Report 92-1, Department of Civil and Environmental Engineering, University of Delaware, DE, 1992.

22. **Chin C.T., Liu C.C.** Volumetric and undrained behaviors of Taipei silty clay. // *Journal of the Chinese Institute of Civil and Hydraulic Engineering*, 1997, Vol. 9, No. 4, pp. 665-678.
23. **Shibata T., Karube D.** Influence of the Variation of the Intermediate Principal Stress on the Mechanical Properties of Normally Consolidated Clays. // *Proceedings of the 6th International Conference on Soil Mechanics and Foundation Engineering*, Montreal, Canada, 1965, Vol. 1, pp. 359-363.
24. **Yong R.N., McKyes E.** Yield and Failure of a Clay Under Triaxial Stresses. // *Journal of the Soil Mechanics and Foundation Division*, ASCE, 1971, Vol. 97, No. SM1, pp. 159-176.
25. **Lade P.V., Musante H.M.** Three-Dimensional Behavior of Remolded Clay. // *Journal of the Geotechnical Engineering Division*, 1978, ASCE, Vol. 104, No. GT2, pp. 193-209.
26. **Nakai T., Matsuoka H., Okuno N., Tsuzuki K.** True Triaxial Tests on Normally Consolidated Clay and Analysis of The Observed Shear Behavior Using Elastoplastic Constitutive Models. // *Soils and Foundations*, 1986, Vol. 26, No. 4, pp. 67-78.
27. **Lade P.V.** Single-Hardening Model with Application to NC Clay. // *Journal of Geotechnical Engineering*, ASCE, 1990, Vol. 116, No. 3, pp. 394-414.
28. **Kirkgard M.M., Lade P.V.** Anisotropic Three-Dimensional Behavior of a Normally Consolidated Clay. // *Canadian Geotechnical Journal*, 1993, Vol. 30, No. 5, pp. 848-858.
29. **Prashant A., Penumadu D.** Effect of Intermediate Principal Stress on Overconsolidated Kaolin Clay. // *Journal of Geotechnical and Geoenvironmental Engineering*, ASCE, 2004, Vol. 130, No. 3, pp. 284-292.
30. **Anantanasakul P., Yamamuro J., Lade P.V.** Three-dimensional drained behavior of normally consolidated anisotropic kaolin clay. // *Soils and Foundations*, 2012, Vol. 52, No. 1, pp. 146-159.
31. **Grim R.E., Bradley R.F.** A Unique Clay form Goose Lake, Illinois Area. // *Journal of the American Ceramic Society*, 1939, Vol. 22, No. 5, pp. 157-164.
32. **Perloff W.H., Osterberg J.O.** The Effect of Strain Rate on the Undrained Shear Strength of Cohesive Soils. // *Proceedings of the Second Pan American Conference on Soil Mechanics and Foundation Engineering*, Sao Paulo, Brasil, 1963, Vol. 1, pp. 103-128.
33. **Kondner R.L., Horner J.M.** Triaxial Compression of a Cohesive Soil with Effective Octahedral Normal Stress Control. // *Canadian Geotechnical Journal*, 1965, Vol. 2, No. 1, pp. 40-52.
34. **Lade P.V., Duncan J.M.** Cubical Triaxial Tests on Cohesionless Soil. // *Journal of the Soil Mechanics and Foundation Division*, ASCE, 1973, Vol. 99, No. SM10, pp. 793-812.
35. **Lade P.V.** Experimental Data for Grundite Clay. Personal communication, 2003.
36. **France J., Sangrey D.A.** Effects of Drainage in Repeated Loading of Clays. // *Journal of Geotechnical Engineering Division*, ASCE, 1977, Vol. 103, No. GT7, pp. 769-785.
37. **Lade P.V.** Stress-Strain Theory for Normally Consolidated Clay. // *Proceedings of the 3rd International Conference on Numerical Methods in Geomechanics*, Aachen, West Germany, 1979, Vol. 1, pp. 1325-1337.

СПИСОК ЛИТЕРАТУРЫ

1. **Kaliakin V.N., Leal A.N., Mashayekhi M.** Modeling the Time- and Temperature-Dependent Response of Cohesive Soils in a Generalized Bounding Surface Framework. // *Transportation Infrastructure Geotechnology*, 2018, Vol. 5, No. 3, pp. 250-286.

2. **Dafalias Y.F.** Bounding Surface Plasticity. I: Mathematical Foundation and the Concept of Hypoplasticity. // *Journal of Engineering Mechanics*, ASCE, Vol. 112, No. 90, 1986, pp. 966-987.
3. **Nieto-Leal A., Kaliakin V.N.** On Soil Yielding and Suitable Choices for Yield and Bounding Surfaces. Report, Department of Civil and Environmental Engineering, University of Delaware, DE, 2013.
4. **Dafalias Y.F.** The Concept and Application of the Bounding Surface in Plasticity Theory. // *IUTAM Symposium on Physical Non-Linearities in Structural Analysis*, Hult J. and Lemaitre J. (Eds.). Springer-Verlag, Berlin, 1981, pp. 56-63.
5. **Nieto-Leal A., Kaliakin V.N.** Improved Shape Hardening Function for Bounding Surface Model for Cohesive Soils // *Journal of Rock Mechanics and Geotechnical Engineering*, 2014, Vol. 6. No. 3, pp. 327-337.
6. **Dafalias Y.F.** An Anisotropic Critical State Soil Plasticity Model. // *Mechanics Research Communications*, 1986, Vol. 13, No. 6, pp. 341-347.
7. **Baker R., Desai C.S.** Induced Anisotropy During Plastic Straining. // *International Journal for Numerical and Analytical Methods in Geomechanics*, 1984, Vol. 8, No. 2, pp. 167-185.
8. **Crouch R.S., Wolf J.P.** On a Three-dimensional Anisotropic Plastic Model for Soil. // *Geotechnique*, 1995, Vol. 45, No. 2, pp. 301-305.
9. **Dafalias Y.F., Herrmann L.R.** Bounding Surface Plasticity II: Application to Isotropic Cohesive Soils. // *Journal of Engineering Mechanics*, ASCE, 1986, Vol. 112, No. 12, pp. 1263-1291.
10. **Dafalias Y.F., Herrmann L.R.** A Bounding Surface Soil Plasticity Model. // *Proceedings of the International Symposium on Soils Under Cyclic and Transient Loading*, Pande G.N. and Zienkiewicz O.C. (Eds.), A.A. Balkema, Rotterdam, 1980, pp. 335-345.
11. **Dafalias Y.F., Herrmann L.R.** Bounding Surface Formulation of Soil Plasticity. // *Soil Mechanics – Transient and Cyclic Loads*, Pande G.N. and Zienkiewicz O.C. (Eds.), John Wiley and Sons, Chichester, UK, Chapter 10, 1982, pp. 253-282.
12. **Kaliakin V.N., Nieto-Leal A.** Details Pertaining to the Generalized Bounding Surface Model for Cohesive Soils. Revised & Expanded, Report, Department of Civil and Environmental Engineering, University of Delaware, DE, 2017.
13. **Kaliakin V.N., Dafalias Y.F.** Simplifications to the Bounding Surface Model for Cohesive Soils. // *International Journal for Numerical and Analytical Methods in Geomechanics*, 1989, Vol. 13, No. 1, pp. 91-100.
14. **Schofield A.N., Wroth C.P.** Critical State Soil Mechanics. McGraw-Hill Book Co., Inc., London, UK, 1968, 310 pages.
15. **Sheng D., Sloan S.W., Yu H.S.** Aspects of finite element implementation of critical state models. // *Computational Mechanics*, 2000, Vol. 26, pp. 185-196.
16. **Kaliakin V.N., Dafalias Y.F.** Theoretical Aspects of the Elastoplastic-Viscoplastic Bounding Surface Model for Cohesive Soils. // *Soils and Foundations*, 1990, Vol. 30, No. 3, pp. 11-14.
17. **Dafalias Y.F.** Bounding Surface Elastoplasticity-Viscoplasticity for Particulate Cohesive Media. // *Deformation and Failure of Granular Materials, IUTAM Symposium on Deformation and Failure of Granular Materials*, Vermeer P.A. and Luger H.J. (Eds.), A.A. Balkema, Rotterdam, 1982, pp. 97-107.
18. **Perzyna P.** Fundamental Problems in Viscoplasticity. // *Advances in Applied Mechanics*, 1966, Vol. 9, pp. 243-377.
19. **Nieto-Leal A.N., Kaliakin V.N., Mashayekhi M.** Improved RH rule for cohesive soils and inherent anisotropy. // *International Journal for Numerical and*

- Analytical Methods in Geomechanics*, 2018, Vol. 42, No. 3, pp. 469-487.
20. **Dafalias Y.F., Manzari M.T., Papadimitriou A.G.** SANICLAY: simple anisotropic clay plasticity model. // *International Journal for Numerical and Analytical Methods in Geomechanics*, 2006, Vol. 30, No. 12, pp. 1231-1257.
 21. **Kaliakin V.N.** CALBR8, A Simple Computer Program for Assessing the Idiosyncrasies of Various Constitutive Models Used to Characterize Soils. Report 92-1, Department of Civil and Environmental Engineering, University of Delaware, DE, 1992.
 22. **Chin C.T., Liu C.C.** Volumetric and undrained behaviors of Taipei silty clay. // *Journal of the Chinese Institute of Civil and Hydraulic Engineering*, 1997, Vol. 9, No. 4, pp. 665-678.
 23. **Shibata T., Karube D.** Influence of the Variation of the Intermediate Principal Stress on the Mechanical Properties of Normally Consolidated Clays. // *Proceedings of the 6th International Conference on Soil Mechanics and Foundation Engineering*, Montreal, Canada, 1965, Vol. 1, pp. 359-363.
 24. **Yong R.N., McKyes E.** Yield and Failure of a Clay Under Triaxial Stresses. // *Journal of the Soil Mechanics and Foundation Division*, ASCE, 1971, Vol. 97, No. SM1, pp. 159-176.
 25. **Lade P.V., Musante H.M.** Three-Dimensional Behavior of Remolded Clay. // *Journal of the Geotechnical Engineering Division*, 1978, ASCE, Vol. 104, No. GT2, pp. 193-209.
 26. **Nakai T., Matsuoka H., Okuno N., Tsuzuki K.** True Triaxial Tests on Normally Consolidated Clay and Analysis of The Observed Shear Behavior Using Elastoplastic Constitutive Models. // *Soils and Foundations*, 1986, Vol. 26, No. 4, pp. 67-78.
 27. **Lade P.V.** Single-Hardening Model with Application to NC Clay. // *Journal of Geotechnical Engineering*, ASCE, 1990, Vol. 116, No. 3, pp. 394-414.
 28. **Kirkgard M.M., Lade P.V.** Anisotropic Three-Dimensional Behavior of a Normally Consolidated Clay. // *Canadian Geotechnical Journal*, 1993, Vol. 30, No. 5, pp. 848-858.
 29. **Prashant A., Penumadu D.** Effect of Intermediate Principal Stress on Overconsolidated Kaolin Clay. // *Journal of Geotechnical and Geoenvironmental Engineering*, ASCE, 2004, Vol. 130, No. 3, pp. 284-292.
 30. **Anantanasakul P., Yamamuro J., Lade P.V.** Three-dimensional drained behavior of normally consolidated anisotropic kaolin clay. // *Soils and Foundations*, 2012, Vol. 52, No. 1, pp. 146-159.
 31. **Grim R.E., Bradley R.F.** A Unique Clay form Goose Lake, Illinois Area. // *Journal of the American Ceramic Society*, 1939, Vol. 22, No. 5, pp. 157-164.
 32. **Perloff W.H., Osterberg J.O.** The Effect of Strain Rate on the Undrained Shear Strength of Cohesive Soils. // *Proceedings of the Second Pan American Conference on Soil Mechanics and Foundation Engineering*, Sao Paulo, Brasil, 1963, Vol. 1, pp. 103-128.
 33. **Kondner R.L., Horner J.M.** Triaxial Compression of a Cohesive Soil with Effective Octahedral Normal Stress Control. // *Canadian Geotechnical Journal*, 1965, Vol. 2, No. 1, pp. 40-52.
 34. **Lade P.V., Duncan J.M.** Cubical Triaxial Tests on Cohesionless Soil. // *Journal of the Soil Mechanics and Foundation Division*, ASCE, 1973, Vol. 99, No. SM10, pp. 793-812.
 35. **Lade P.V.** Experimental Data for Grundite Clay. Personal communication, 2003.
 36. **France J., Sangrey D.A.** Effects of Drainage in Repeated Loading of Clays. // *Journal of Geotechnical Engineering Division*, ASCE, 1977, Vol. 103, No. GT7, pp. 769-785.

37. **Lade P.V.** Stress-Strain Theory for Normally Consolidated Clay. // *Proceedings of the 3rd International Conference on Numerical Methods in Geomechanics*, Aachen, West Germany, 1979, Vol. 1, pp. 1325-1337.
-

Victor N. Kaliakin, Professor, Ph.D., Department of Civil & Environmental Engineering, University of Delaware, 19716, USA; phone +1(302)831-2409 (office); fax +1(302)831-3640; E-mail: kaliakin@udel.edu.

Andres Nieto-Leal, Assistant Professor, Ph.D., Chairman, Department of Civil Engineering, Universidad Militar Nueva Granada, Cajica, 250247, Colombia; e-mail: andres.nieto@unimilitar.edu.co.

Калякин Виктор Н., профессор, доктор наук; Департамент гражданского и экологического инжиниринга, Университет штата Делавэр, г. Ньюарк, США; тел. +1(302) 831-2409; факс +1(302)831-3640; e-mail: kaliakin@udel.edu.

Андрес Ньето-Лил, доцент, доктор наук, Департамент гражданского строительства, Университет Милитара Нуэва, Гранада, Кахика, 250247, Колумбия; E-mail: andres.nieto@unimilitar.edu.co.